PCCP

Accepted Manuscript




ROYAL SOCIETY OF CHEMISTRY

www.rsc.org/pccp

Submitted to PCCP, 1/16/2013

# Nine-dimensional global potential energy surface for $NH_4(X^2A_1)$ and kinetics studies on the $H + NH_3 \leftrightarrow H_2 + NH_2$ reaction

Jun Li and Hua Guo*

*Department of Chemistry and Chemical Biology, University of New Mexico, Albuquerque, New Mexico 87131, USA*

*TOC graphic*

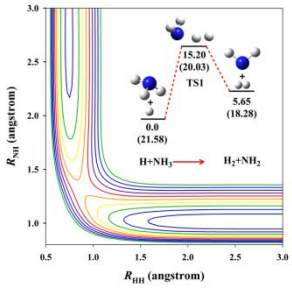


*A nine-dimensional global potential energy surface (PES) for the $NH_4$ system is developed from ~$10^4$ high-level ab initio points and the hydrogen abstraction kinetics on the PES agree with experiment.*

*: corresponding author, email: hguo@unm.edu

## Abstract

Extensive *ab initio* calculations of the stationary points in the $NH_4(X^2A_1)$ system are reported using both coupled cluster and multi-reference configuration interaction methods. In addition, more than 100,000 points are generated over a large configuration space and energy range (6eV) using the explicitly correlated unrestricted coupled cluster method with singles, doubles, and perturbative triples excitations with the augmented correlation-consistent polarized triple zeta basis set (UCCSD(T)-F12a/aug-cc-pVTZ). Using the recently proposed permutation-invariant polynomial neural network (PIP-NN) method, these points are accurately fit to an analytical form with a total root mean squared error (RMSE) of 3.4 meV (0.08 kcal/mol). Both the abstraction and exchange channels as well as the metastable ammonium radical ($NH_4$) are included in this potential energy surface. Transition-state theory and quasi-classical trajectory calculations have been performed to obtain the rate constants for the abstraction reaction and its reverse. Comparison with available experimental results is satisfactory, providing supporting evidence for the accuracy of the potential.

## I. Introduction

An exciting current development in the field of quantum reaction dynamics is a shift of focus from atom-diatom type reactions to reactions involving polyatomic systems.[1-4] The latter, which have also been extensively investigated experimentally,[5-6] often involve more complex and interesting dynamics, but at the same time more demanding for a quantum mechanical characterization as the size of the problem increases exponentially with the number of degrees of freedom. Nevertheless, significant progress has recently been made for reactions involving four atoms, for which full-dimensional quantum dynamics on accurate global potential energy surfaces (PESs) have become possible.[7-15] These advances have shed valuable lights on an array of important dynamical issues such as tunneling, resonances, mode specificity, and non-adiabatic effects, as exemplified by two recent theory-experimental studies.[16-17] To move beyond tetra-atomic reactions, penta-atomic systems with nine internal degrees of freedom become the natural choice. We note that there have been two full-dimensional quantum dynamical studies for such systems already,[18-19] and more are to be expected in the near future. A major obstacle for an reliable characterization of penta-atomic reactions is the accurate representation of the nine-dimensional global PES, without which the dynamical calculations cannot possibly be expected to yield correct results.

The $NH_4$ system presents an ideal proving ground for quantum mechanical characterization of its spectroscopy and reaction dynamics, as it has a small number of electrons (11) and four hydrogen atoms. The former affords a high-level *ab initio* treatment of the electronic structure, while the latter permits a relatively small basis/grid for the quantum dynamical calculations. On the ground electronic state of $NH_4(X^2A_1)$, there are two major reaction channels. One is the abstraction reaction:

$$H + NH_3 \leftrightarrow H_2 + NH_2 \qquad \Delta H_{rxn}(0K)=2.7 \text{ kcal/mol} \qquad (R1)$$

and the other is the exchange reaction via the $NH_4$ intermediate:

$$H + NH_3 \leftrightarrow NH_4 \leftrightarrow H + NH_3 \qquad \Delta H_{rxn}(0K)=0 \text{ kcal/mol} \qquad (R2)$$

The metastable ammonium radical ($NH_4$) cannot dissociate into $H_2(X^1\Sigma_g^+)$ and $NH_2(X^2B_1)$ on the ground electronic state and an excited state has to be involved.[20]

Earlier theoretical characterizations of this system were mostly concerned with the reactive transition state of the abstraction reaction (R1).[21-24] Global PESs for the ground electronic state of $NH_4$ has later been developed by several authors. In 1997, Corchado and Espinosa-Garcia (CE-1997) reported the first analytical PES for the reaction R1 in this system based on both *ab initio* and experimental data,[25] but it was later found to have an unphysical description for the $NH_3$ inversion. This PES was improved in 2010 (CE-2010) exclusively based on *ab initio* data with the inversion problem fixed.[26] However, neither includes the exchange channel (R2). In 2005, Moyano and Collins (MC) developed a global PES using the modified Shepard interpolation method based on *ab initio* information at 2000 points obtained at the unrestricted couple-cluster singles, doubles and perturbative triples with the augmented correlation-consistent polarized valence triple zeta basis set (UCCSD(T)/aug-cc-pVTZ) level.[27] The MC PES includes both the R1 and R2 pathways, which is important for a realistic representation of the global PES as the R1 barrier is higher than that for R2, but oscillations in the frequencies and consequently the vibrational adiabatic plots along the reaction path of the reaction R1 were found.[28] Both the CE and MC PESs have been used in quasi-classical trajectory (QCT)[27-29] and quantum mechanical (QM) studies.[19, 30-34]

Although there has been no experimental study of the dynamics of either R1 or R2, the kinetics of R1 and its reverse have been extensively investigated through various techniques, due to its importance in combustion of nitrogen-containing species. Rate constants have been reported for both R1[35-42] and its reverse (R-1),[41, 43-45] including kinetic isotope effects.

While no rate constants for R2 have been reported, there has been intensive interest in the ammonium radical in the R2 reaction pathway. The identification of this metastable species was first made by Herzberg,[46] who attributed the Schüler emission bands in ammonia discharge to transitions in this Rydberg molecule.[47] The ground state radical has very short lifetime, due apparently to tunneling facilitated decay.[48-49] Taking advantage of the much longer lifetime, spectroscopic analyses of the deuterated ammonium radical ($ND_4$) have been carried out.[46, 50-53] Very recently, there is a renewed interest on this species, particularly on the unimolecular decay dynamics.[54] These experimental activities have stimulated theoretical characterizations of this species.[55-58]

From the aforementioned survey, it is clear that the existing PESs for the $NH_4$ system are inadequate to give a uniformly accurate description of both R1 and R2. As a result, it is highly desirable to develop a globally accurate PES based on a large number of high-level *ab initio* calculations, which can be used for both QCT and QM studies of reaction dynamics as well as spectroscopy. The PES should satisfy several key requirements. First, it must be based on chemically accurate electronic structure theory, which is typically defined as errors < 1 kcal/mol. Second, it needs to cover all relevant configuration space, including the reaction asymptotes, transition states, and potential wells. Third, it should possess the correct permutation symmetry of this system where four of five atoms in the system are indistinguishable. Finally, it has to have minimal fitting errors. To answer these challenges, we report here a new full-dimensional PES

based on ~103,000 high-level *ab initio* points, using the permutation invariant polynomial-neural network (PIP-NN) method recently proposed by us.[59-60] It is shown that the PES provides a faithful representation of the *ab initio* points with a total root mean squared error (RMSE) of 3.4 meV (0.08 kcal/mol). To test the PES, we have carried out reaction path analysis and computed the rate constants for R1 and R-1 using both transition-state theory and QCT.

## II. *Ab initio* calculations

The geometries for all the stationary points were optimized at the levels of FC-UCCSD(T)-F12a/aug-cc-pVnZ (n = D, T), and AE-UCCSD(T)-F12b/cc-pCVnZ-F12 (n = D, T, and for some species Q). FC and AE stand for "frozen-core" and "all-electron" treatments in the post-Hartree-Fock calculations, respectively. Aug-cc-pVTZ or AVTZ denotes the augmented correlation-consistent polarized valence triple-zeta basis set,[61] and cc-pCVnZ-F12 the basis sets optimized for accurate description of the core-core and core-valance correlation effects with explicitly correlated (F12) methods.[62] These F12 versions of the CCSD(T)[63-64] have been shown to yield atomization energies, electron affinities, ionization potentials, equilibrium geometries, and harmonic frequencies for both close- and open-shell systems better than CCSD(T) with the augmented correlation-consistent polarized valence quintuple-zeta (AV5Z) basis set,[65] and recommended for developing PESs.[66] All calculations have been carried out using MOLPRO 2010.1.[67]

As shown in Table I, the geometric parameters of stationary points obtained at different levels of theory are all consistent with each other and are in general agreement with available experimental and other high-level *ab initio* results. The differences in bond lengths are generally within 0.003Å, angles within 0.5°. The good agreement suggests that the effect of the core

electrons is negligible, and the results have also converged with respect to the basis size. Consequently, the FC-UCCSD(T)-F12a/AVTZ level of theory was selected, as a compromise between efficiency and costs, for computing the energies of the PES points.

For the metastable $NH_4$ radical, some additional tests were performed. Its geometry was first optimized at the levels of FC-UCCSD(T)/VTZ and VQZ, which was used to calibrate the CE-2010 (although this channel was not included in that PES). As shown in Table I, although the $T_d$ symmetry is maintained, the N-H bond lengths of 1.0520 and 1.0457 Å are much larger than the experimental derived value of 1.0365 Å,[53] or 1.0355/1.0388 Å obtained at the complete basis set (CBS) limit FC-CCSD(T)/CBS (Ref. 58)/FC-CCSD(T)-F12a/AVTZ (this work) levels. We have also carried out Davidson corrected[68] multi-reference configuration interaction (MRCI+Q(FV+3s)) calculations[69] with the AVDZ and AVTZ basis sets, but the N-H bond length (1.0494 and 1.0425 Å, respectively) was also longer than both experimental and CCSD(T) values, as shown in Table I.

In Fig. 1, the energetics and geometries of stationary points in both reaction pathways are shown. At the FC-UCCSD(T)-F12a/AVTZ level of theory, the abstraction transition state (TS1) leading to $NH_2$ and $H_2$ is 15.20 kcal/mol above the reactant asymptote. The classical reaction energy of the abstraction channel, 5.65 kcal/mol, is 0.33 kcal smaller than the benchmark value 5.98 by the HEAT protocol,[70] which has an average error within 1 kJ/mol. It becomes 2.35 kcal/mol with zero-point energy (ZPE) correction within the harmonic oscillator approximation at the FC-UCCSD(T)-F12a/AVTZ level, or 2.66 kcal/mol with ZPE corrected with anharmonic contributions in the HEAT protocol,[70] respectively. The transition state for the formation of $NH_4$ along the exchange channel (TS2) is 9.39 kcal/mol above the same reactant asymptote. In addition to these reactive transition states, ammonia $NH_3$ has a planar inversion transition state

(denoted as $NH_3$-TS, classically 5.24 kcal/mol), which is not shown in Fig. 1 but included in Table I.

The corresponding harmonic frequencies of the stationary points at various levels of theory are compared in Table II. They are also consistent with each other. It is noteworthy again that at the FC-UCCSD(T)/VTZ or VQZ level, the harmonic frequencies of $NH_4$ are quite different from other *ab initio* results. This suggests that the inclusion of augmented basis functions is important for this Rydberg system. The calculated harmonic frequencies of the $NH_4$ are consistent with the experimental values,[49] although there are some uncertainties in the latter.

For comparison, the corresponding information of the stationary points on the CE-2010 PES[26] is also included in Table I. It is clear that there are significant differences between that PES and our benchmark *ab initio* values for almost all stationary points. In particular, we note that the collinear $\theta_{NH'H''}$ angle of the CE-2010 TS1 is in strong contrast to the bent geometry (159.96°) predicted by the *ab initio* calculations. In addition, the comparison of the harmonic frequencies in Table II also reveals substantial differences between CE-2010 PES and our *ab initio* data. At $NH_3$-TS, for example, all five real harmonic frequencies are about 200 $cm^{-1}$ different from our *ab initio* values. These discrepancies indicate that the CE PESs are not quantitatively accurate.

Although the $T_1$ diagnostics test[71] of the stationary points suggests predominantly single reference nature, we were interested in finding out the performance of multi-reference methods such as MRCI for this system. To this end, we have carried out MRCI calculations with different basis sets and active spaces at the geometries optimized at the level of FC-UCCSD(T)-F12a/AVTZ. The results are compared in Table III. If only the full valence (FV) active space is

considered, energies for TS1 and the abstraction products $NH_2 + H_2$ were underestimated by ~3.5 kcal/mol, and those for TS2 and $NH_4$ were underestimated by ~2.0 and ~1.3 kcal/mol, respectively, compared to those at the level of FC-UCCSD(T)-F12a/AVTZ, although the basis set effect is marginal. Once the 3s orbital of N is included in the active space (FV+3s), the results are significantly improved, and converged with the AVQZ basis set. Noteworthy, the MRCI+Q(FV+3s) calculation with the averaged atomic natural orbitals (ANOs)[72] gives results similar to those at the level of MRCI+Q(FV+3s)/CBS, which is extrapolated from AVTZ and AVQZ results. The addition of the 3p orbital to the active space, (FV+3s3p), makes the calculation much more expensive, but its effect on the results is small. The MRCI approach was not pursued because it is significantly more expensive than the CCSD(T) calculations.

The intrinsic reaction coordinate (IRC) analyses of the three transition states were performed at the level of FC-UCCSD(T)-F12a with two basis sets, AVTZ and/or AVDZ. The results are compared in Fig. 2 and one can see that the difference between the two basis sets is negligible, except for $NH_4$, where the energy with AVDZ is ~0.2 kcal/mol lower than that with AVTZ.

**III. Potential energy surface**

In order to build a globally accurate PES with reasonable computational costs, especially for such a high-dimensional system, it is vital to sample the *ab initio* points prudently. Our strategy is similar to that in our recent work on the HOCO and $XH_2O$ (X=F,O,Cl) systems.[73-78] First, stationary points were surveyed to determine the ranges of configurations and energies. In this work, we discarded points with energies higher than 6 eV (138.4 kcal/mol), relative to the reactant asymptote ($H + NH_3$), in order to guarantee accuracy in high temperature simulations of

rate constants. Second, we used grids with appropriate coordinates in various regions to sample relevant configurations. In the reactant region, for instance, the internal coordinates of $NH_3$ were sampled in fine grids while the coordinates involving the attaching H atom were sampled in relative sparse grids. The resulting PES was then validated by comparing with key *ab initio* properties of stationary points and asymptotes, such as geometries and energies. Furthermore, batches of trajectories at various energies were dispatched to search for unphysical regions of the PES resulted from the lack of *ab initio* data points. New points were then added to patch up these regions if they are not close to existing data sets. This was judged by the Euclidean distance defined in terms of the bond lengths between any point $\{\vec{r}_i\}$ and a data point $\{\vec{r}_i'\}$ in the existing data sets, $\chi(r_i) = \sqrt{\sum_i^{10} |\vec{r}_i - \vec{r}_i'|} < 0.1$ Å. All permutation equivalent points are included in such screening. This procedure was iterated multiple times until the results converged. To make sure of the validity of the CCSD(T) method, those points with $T_1$ values larger than 0.05, which constitute only a very small percentage of points calculated, were discarded. Finally, ~103,000 points were obtained at the FC-UCCSD(T)-F12a/AVTZ level, and used to construct the PES.

To provide an analytical representation of these *ab initio* points, we used the permutation invariant polynomial-neural network (PIP-NN) method proposed recently by us.[59-60] The fitting of global PESs using NN has been in existence in some time,[79-81] and recent applications to reactive PESs have shown impressive results.[10, 59-60, 82] Specifically, an NN converts a signal (*e.g.*, geometry) in the form of an input vector ($\mathbf{G} = \{G_i\}$) to a scalar output (*E*, *i.e.* potential energy) *via* one or more hidden layers of interconnecting neurons. The non-linear nature of NNs provides a flexible means to approximate any unknown real-valued multi-dimensional function accurately. The non-linear parameters defining the NN are obtained by "training" with the data set. Our PIP-

NN approach[59-60] enforces permutation symmetry in the NN fitting by employing a special set of symmetry functions as the input vector, rather than the geometries themselves. The symmetry functions are PIPs of Morse variables defined in terms of internuclear distances, as introduced by Bowman and coworkers.[83-84] An important point in PIP-NN fitting of PESs with four or more atoms is that more PIPs than the internal coordinates are needed to ensure permutation invariance.[60] The PIP-NN method has been used to fit PESs for tri- and tetra-atomic systems where the number of points are far less than the one reported here.[59-60]

In this first PIP-NN fit of a five-atom system, the maximum total order of the PIPs in the input vector is four, resulting in 81 PIPs. In the NN fitting, the data were divided randomly into three sets, namely the training (90%), validation (5%), and test (5%) sets. To avoid false extrapolation due to edge points in the randomly selected validation and test sets, only fits with similar RMSEs (defined as $\mathrm{RMSE}=\sqrt{\sum_{i=1}^{N_{\mathrm{data}}}\left(E_{\mathrm{output}}-E_{\mathrm{target}}\right)^2/N_{\mathrm{data}}}$) for all three sets were accepted. In addition, the maximum deviation is also used in selecting the final PIP NN PESs. Different NN architectures with two hidden layers were tested. For each architecture, 50 different training calculations were performed and the "early stopping" method[81] was used to avoid overfitting. The training converged fast for all the fitting reported here, typically finishing within a few hundred steps. The final PIP-NN PES was chosen as the average of three best PES to minimize random errors. As a compromise between efficiency and costs, a two-layer NN with 20 and 80 neurons in each layer was chosen, which has 3421 parameters. The RMSEs for the train/validation/test sets and maximum deviation of the three best PESs are 3.6/4.3/4.9/162.5, 4.9/5.8/6.0/152.2, and 3.7/5.0/6.1/154.7 meV, respectively. The final PES has a total RMSE of 3.4 meV and a maximum deviation of 108.6 meV. The fitting errors of all the data points are

shown in Fig. 3 as a function of energy. It is remarkable that the small errors are relatively evenly distributed in the entire energy range. The PES can be obtained from the author (HG) upon request.

The properties of the stationary points on the PIP-NN PES are listed in Tables I, II, and III, and the geometries, harmonic frequencies, and energies are all in excellent agreement with those calculated at the target level (FC-UCCSD(T)-F12a/AVTZ). To further illustrate the accuracy of the fit, the intrinsic reaction paths associated with the three saddle points are compared with the *ab initio* results in Figure 2.

In Fig. 4, two one-dimensional cuts of the PES are compared with the *ab initio* data. In the first, the dependence of TS1 on the NHH' angle is shown and it is clear that the saddle point is away from the linearity, see also Table I and above discussion. The second curve follows the dissociation of $NH_4$ to the H + $NH_3$ channel with other coordinates fixed at the equilibrium geometry of $NH_4$. The barrier, which is responsible to the tunneling facilitated decay of the metastable $NH_4$ and $ND_4$, are clearly visible. In both cases, it is clear that the PES provides a faithful representation of the *ab initi*o points.

Since the earlier CE-1997 PES suffered from a poor description of the $NH_3$ inversion in the reactant asymptote,[26] special attention has been paid to this region. The tunneling splitting of $NH_3$ was computed using a full-dimensional quantum method described elsewhere.[85] The result (1.07 $cm^{-1}$) and the agreement with known experimental value (0.79 $cm^{-1}$) is satisfactory, indicating a good description of the inversion barrier.

In Fig. 5, the PES is plotted as a function of the breaking and forming bondlengths ($r_{NH}$ and $r_{HH}$) for the abstraction reaction, while all other coordinates are optimized. It is clear that the

transition state is "late", consistent with the geometry of TS1 in Fig. 1 and Table I.

## IV. Reaction path analysis and kinetics calculations

The reaction path Hamiltonian[86] for the abstraction reaction (R1) was determined on the PIP-NN PES using POLYRATE 9.7,[87] starting from the saddle point geometry and going downhill to both sides in mass-weighted Cartesian coordinates using Page and McIver's method[88] with a step size of 0.00094 amu$^{1/2}$•bohr. Along the minimum energy path (MEP), the reaction coordinate ($s$) is defined as the signed distance from the saddle point ($s$=0), with $s$>0 referring to the product side and $s$<0 to the reactant side. The reaction path was followed between $s$=-2.2 and $s$=2.2 amu$^{1/2}$•bohr and the Hessian matrix was calculated every 10 points. These parameters have been tested for convergence. All calculations were carried out in mass-scaled coordinates with a reduced mass equal to 1 amu. Along the MEP, a generalized normal-mode analysis was performed using a redundant curvilinear projection formalism[89] by projecting these modes along the reaction path as well as overall rotations and translations. With such information, the vibrationally adiabatic potentials were determined: $V_a(n,s) = V_{\mathrm{MEP}}(s) + \varepsilon_{\mathrm{int}}(n,s)$, where $V_{\mathrm{MEP}}(s)$ is the potential energy along the MEP with its zero at the reactants, and $\varepsilon_{\mathrm{int}}(n,s)$ is the vibrational energy at $s$ from the generalized normal-mode vibrations orthogonal to the reaction coordinate. $V_a(n=0, s)$ corresponds to the ground vibrational state adiabatic potential, $V_a^G(s)$.

The reaction path curvature has the components $B_{m\mathrm{F}}(s)$, the coupling terms between the $m$th generalized normal mode and the reaction coordinate, mode $F$, $\kappa(s) = \left( \sum_{m=1}^{F-1} \left[ B_{mF}(s) \right]^2 \right)^{1/2}$, and these coupling terms control the non-adiabatic flow of energy between these vibrational modes

and the reaction coordinate. These coupling terms were used in the calculation of transmission coefficients that include the effects of the reaction path curvature.

Figure 6 shows the classical MEP ($V_{MEP}$), vibrationally adiabatic ground state energy ($V_a^G$), ZPE, generalized normal mode frequencies, and the curvature ($\kappa$) as a function of the reaction coordinate $s$. The classical barrier at the PES saddle point is 15.11 kcal/mol at $s$=0.0 amu$^{1/2}$bohr, but the maximum of $V_a^G(s)$ (13.99 kcal/mol with respect to the reactant asymptote) is shifted to $s$=+0.09 amu$^{1/2}$bohr. This is indicative of a variational effect for this system. As shown in the figure, there are six $NH_3$ modes with the large frequencies in reactant asymptote. In the vibrationally adiabatic picture, the symmetric stretching (labeled 3) frequency gradually decreases to 1576 cm$^{-1}$ at $s$=-0.17 amu$^{1/2}$bohr, as the two reactants approach each other. The significant change in ZPE around the TS is responsible for the shifted maximum in $V_a^G(s)$ along $s$. There are two peaks in $\kappa$ before and after the saddle point, as often seen in thermo-neutral reactions.

The rate constants for both R1 and R-1 and their fully deuterated counterparts were computed using the canonical variational transition-state theory (CVTST, or CVT).[90] Quantum effects for motions transverse to the reaction path were included by using quantum mechanical vibrational partition functions under the harmonic approximation, while quantum effects in the reaction coordinate were included by using the micro-canonical optimized multidimensional tunneling (μOMT) approach,[90] in which, at each total energy, the larger of the small-curvature (SCT) and large-curvature (LCT) tunneling probabilities was taken as the best estimate. The rotational partition functions were calculated classically.

The results are compared with available experimental results in Figs. 7 and 8. The

agreement are quite good, providing evidence for the accuracy of the PES, particularly for the area near the transition state. In Table IV, kinetic isotope effects are compared with both experiment and theoretical values obtained on the earlier PESs. The theoretical results are consistent with the experiment and with each other, and they indicate significant tunneling.

The rate constants were also computed for the H + $NH_3$ → $H_2$ + $NH_2$ reaction using the standard QCT method implemented in VENUS.[91] Batches ($10^5$~$10^6$) of trajectories were calculated at the temperatures 1000, 1500, 2000, and 2500 K to make the statistical errors all within 3.5% except for the temperature 1000K with 5.2% error. No QCT calculations were attempted at lower temperatures due to very low reactivity. The initial ro-vibrational energies of $NH_3$ and translational energies between H and $NH_3$ were sampled according to the Boltzmann distribution at each specific temperature.[92] The maximal impact parameter ($b_{max}$) was determined using small batches of trajectories with trial values at each temperature. The trajectories were initiated with a reactant separation of 6.0 Å, and terminated when products reached a separation of 6.0 Å, or when reactants are separated by 6.0 Å for non-reactive trajectories. During the propagation, the gradient of the PES was obtained numerically by a central-difference algorithm. The propagation time step was selected to be 0.01 fs, which conserves the energy better than $10^{-4}$ kcal/mol for all trajectories in this work. A few trajectories which were nonreactive after 10.0 ps were discarded. The rate constant was calculated as follows $k_1 = \sqrt{\frac{8k_BT}{\pi\mu}}\pi b_{max}^2 \frac{N_r}{N_{total}}$, in which $N_r$ and $N_{total}$ are the numbers of reactive and total trajectories and μ is the reduced mass for the reactant channel. The results are compared with the CVT results and as shown in Fig 7a, and the agreement is satisfactory. However, we note that the product state ZPEs were not included in computing the rate constants, which can lead to a large uncertainty in the calculated results

because of the small endothermicity of the reaction and the large ZPE of the products.

## V. Mode selectivity

Although we report no dynamical calculations using the new PIP-NN PES, it is possible to predict mode selectivity using our newly proposed Sudden Vector Projection (SVP) model.[93-95] The SVP model is based on the premise that the reaction occurs at the sudden limit where energy flow is significantly slower than the collision time. In addition, the ability of a reactant mode to promote the reaction is quantified by the projection of the corresponding normal mode vector ($\vec{Q}_i$, $i$ corresponds to vibrational, rotational and translation modes) onto the reaction coordinate vector at the transition state ($\vec{Q}_{RC}$). This model has been successfully applied to several gas phase and surface reactions[93-97] and is particularly suited for the current one because of the low density of states in the system.

The calculated SVP values ($P_i = \vec{Q}_i \cdot \vec{Q}_{RC} \in [0,1]$) for both the reactants and products of R1 are listed in Table V. It is shown that both the symmetric and antisymmetric stretching modes of $NH_3$ are expected to promote the reaction, judging from their large $P_i$ values. This is readily understandable as TS1 (Fig. 1) features a stretched N-H bond in the $NH_3$ moiety. These modes are followed by the umbrella and bending modes of $NH_3$. These predictions are consistent with the previous quantum dynamical calculations of Yang and Corchado.[32] Although the CE-1997 PES was used in that calculation, its transition state is sufficiently close to the PIP-NN PES.

The product energy disposal in R1 is also predicted by the SVP model (Table V), which suggests that the product $H_2$ is expected to be vibrationally excited while $NH_2$ is vibrationally cold and hence might be considered a spectator. Invoking microscopic reversibility, these SVP

values imply that the $H_2$ vibration would promote the R-1 reaction whereas the vibrational excitation of $NH_2$ has a limited effect. These predictions are also consistent with the 7-dimensional quantum dynamical study of Yang and Corchado.[31, 34]

## VI. Conclusions

In this work, we present a globally accurate 9D PES for the ground electronic state of $NH_4$. It contains both abstraction and exchange reaction channels as well as the potential well for the ammonium radical. The PES is based on a large number of "gold standard" coupled cluster points over a large configuration space, and the fit preserves the permutation symmetry of the system and has an extremely small fitting errors. As a result, this PES provides a reliable platform on which both spectroscopy and reaction dynamics can be determined. Indeed, calculations of rate constants using both TST and QCT methods have yielded good agreement with experimental data for the abstraction reaction. Based on our new PES, mode selectivity for the abstraction reaction and its reverse is also predicted using the SVP model. It is our hope that the current work will stimulate both experimental and theoretical activities on this prototypical system.

**Acknowledgements**: This work was supported by the Department of Energy (DE-FG02-05ER15694). We thank Prof. Minghui Yang for many discussions and Dr. Jianyi Ma for help on the calculation of the tunneling splitting of the $NH_3$.

References:


1 S. C. Althorpe and D. C. Clary, Annu. Rev. Phys. Chem. **54**, 493 (2003).
2 U. Manthe, Mole. Phys. **109**, 1415 (2011).
3 H. Guo, Int. Rev. Phys. Chem. **31**, 1 (2012).
4 G. Nyman and H.-G. Yu, Int. Rev. Phys. Chem. **32**, 39 (2012).
5 N. Balucani, G. Capozza, F. Leonori, E. Segoloni and P. Casavecchia, Int. Rev. Phys. Chem. **25**, 109 (2006).
6 K. Liu, Adv. Chem. Phys. **149**, 1 (2012).
7 D. H. Zhang, M. A. Collins and S.-Y. Lee, Science **290**, 961 (2000).
8 D. H. Zhang, D. Xie and M. Yang, Phys. Rev. Lett. **89**, 283203 (2002).
9 B. Fu and D. H. Zhang, J. Chem. Phys **138**, 184308 (2013).
10 J. Chen, X. Xu, X. Xu and D. H. Zhang, J. Chem. Phys. **138**, 221104 (2013).
11 F. Matzkies and U. Manthe, J. Chem. Phys. **108**, 4828 (1998).
12 B. Jiang, D. Xie and H. Guo, J. Chem. Phys. **135**, 084112 (2011).
13 J. Ma, J. Li and H. Guo, J. Phys. Chem. Lett. **3**, 2482 (2012).
14 J. Li, B. Jiang and H. Guo, J. Am. Chem. Soc. **135**, 982 (2013).
15 J. Li, B. Jiang and H. Guo, Chem. Sci. **4**, 629 (2013).
16 C. Xiao, X. Xu, S. Liu, T. Wang, W. Dong, T. Yang, Z. Sun, D. Dai, X. Xu, D. H. Zhang and X. Yang, Science **333**, 440 (2011).
17 R. Otto, J. Ma, A. W. Ray, J. S. Daluz, J. Li, H. Guo and R. E. Continetti, Science **343**, 396 (2014).
18 D. Wang, J. Chem. Phys. **124**, 201105 (2006).
19 M. Yang, J. Chem. Phys. **129**, 064315 (2008).
20 J. K. Park, J. Chem. Phys. **109**, 9753 (1998).
21 M. S. Gordon, D. R. Gano and J. A. Boatz, J. Am. Chem. Soc. **105**, 5771 (1983).
22 B. C. Garrett, M. L. Koszykowski, C. F. Melius and M. Page, J. Phys. Chem. **94**, 7096 (1990).
23 E. Kraka, J. Gauss and D. Cremer, J. Chem. Phys. **99**, 5306 (1993).
24 J. Espinosa-Garcia and J. C. Corchado, J. Chem. Phys. **101**, 1333 (1994).
25 J. C. Corchado and J. Espinosa-Garcia, J. Chem. Phys. **106**, 4013 (1997).
26 J. Espinosa-Garcia and J. C. Corchado, J. Phys. Chem. A **114**, 4455 (2010).
27 G. E. Moyano and M. A. Collins, Theo. Chem. Acc. **113**, 225 (2005).
28 J. C. Corchado, J. Espinosa-Garcia and M. H. Yang, J. Chem. Phys. **135**, 014303 (2011).
29 J. Espinosa-Garcia and J. C. Corchado, J. Phys. Chem. A **114**, 6194 (2010).
30 H. Li, X. G. Liu and Q. G. Zhang, Chin. Phys. Lett. **22**, 1093 (2005).
31 M. Yang and J. C. Corchado, J. Chem. Phys. **127**, 184308 (2007).
32 M. Yang and J. C. Corchado, J. Chem. Phys. **126**, 214312 (2007).
33 X. Q. Zhang, Q. Cui, J. Z. H. Zhang and K. L. Han, J. Chem. Phys. **126**, 234304 (2007).
34 Y. Yang, R. Liu, R. Wan and M. Yang, J. Theo. Comput. Chem. **12**, 1350054 (2013).
35 C. Willis, A. W. Boyd and O. A. Miller, Can. J. Chem. **47**, 3007 (1969).
36 J. E. Dove and W. S. Nip, Can. J. Chem. **52**, 1171 (1974).
37 M. Yumura, T. Asaba, Y. Matsumoto and H. Matsui, Inter. J. Chem. Kinet. **12**, 439 (1980).
38 J. V. Michael, J. W. Sutherland and R. B. Klemm, Int. J. Chem. Kinet. **17**, 315 (1985).
39 P. Marshall and A. Fontijn, J. Chem. Phys. **85**, 2637 (1986).
40 P. Marshall and A. Fontijn, J. Phys. Chem. **91**, 6297 (1987).
41 J. W. Sutherland and J. V. Michael, J. Chem. Phys. **88**, 830 (1988).
42 T. Ko, P. Marshall and A. Fontijn, J. Phys. Chem. **94**, 1401 (1990).
43 M. Demissy and R. Lesclaux, J. Am. Chem. Soc. **102**, 2897 (1980).
44 W. Hack, P. Rouveirolles and H. G. Wagner, J. Phys. Chem. **90**, 2505 (1986).
45 G. Friedrichs and H. G. Wagner, Z. Phys. Chem. **214**, 1151 (2000).
46 G. Herzberg, Faraday Discuss. **71**, 165 (1981).
47 H. Schüler, A. Michel and A. E. Grun, Z. Naturforsch. A **10**, 1 (1955).
48 G. I. Gellene, D. A. Cleary and R. F. Porter, J. Chem. Phys. **77**, 3471 (1982).
49 G. Herzberg, J. Astrophys. Astron. **5**, 131 (1984).
50 F. Alberti, K. P. Huber and J. K. G. Watson, J. Mol. Spectrosc. **107**, 133 (1984).

51 J. K. G. Watson, J. Mol. Spectrosc. **107**, 124 (1984).
52 E. A. Whittaker, B. J. Sullivan, G. C. Bjorklund, H. R. Wendt and H. E. Hunziker, J. Chem. Phys. **80**, 961 (1984).
53 R. Signorell, H. Palm and F. Merkt, J. Chem. Phys. **106**, 6523 (1997).
54 J. D. Savee, J. E. Mann and R. E. Continetti, J. Phys. Chem. Lett. **4**, 3683 (2013).
55 J. Kaspar, V. H. Smith and B. N. McMaster, Chem. Phys. **96**, 81 (1985).
56 J. K. Park, J. Chem. Phys. **107**, 6795 (1997).
57 F. W. Chen and E. R. Davidson, J. Phys. Chem. A **105**, 10915 (2001).
58 K. W. Sattelmeyer, H. F. Schaefer and J. F. Stanton, J. Chem. Phys. **114**, 9863 (2001).
59 B. Jiang and H. Guo, J. Chem. Phys. **139**, 054112 (2013).
60 J. Li, B. Jiang and H. Guo, J. Chem. Phys. **139**, 204103 (2013).
61 R. A. Kendall, T. H. Dunning and R. J. Harrison, J. Chem. Phys. **96**, 6796 (1992).
62 J. G. Hill, S. Mazumder and K. A. Peterson, J. Chem. Phys. **132**, 054108 (2010).
63 T. B. Adler, G. Knizia and H.-J. Werner, J. Chem. Phys. **127**, 221106 (2007).
64 G. Knizia, T. B. Adler and H.-J. Werner, J. Chem. Phys. **130**, 054104 (2009).
65 D. Feller and K. A. Peterson, J. Chem. Phys. **139**, 084110 (2013).
66 G. Czakó, I. Szabó and H. Telekes, J. Phys. Chem. A **118**, 646 (2014).
67 MOLPRO is a package of ab initio programs written by H.-J. Werner and P.J. Knowles with contributions from G. Knizia et al.
68 S. R. Langhoff and E. R. Davidson, Int. J. Quant. Chem. **8**, 61 (1974).
69 H.-J. Werner, Adv. Chem. Phys. **69**, 1 (1987).
70 A. Tajti, P. Szalay, A. G. Császár, M. Kállay, J. Gauss, E. F. Valeev, B. A. Flowers, J. Vázquez and J. F. Stanton, J. Chem. Phys. **121**, 11599 (2004).
71 T. J. Lee, Chem. Phys. Lett. **169**, 529 (1990).
72 P.-O. Widmark, P.-Å. Malmqvist and B. Roos, Theo. Chim. Acta **77**, 291 (1990).
73 J. Li, Y. Wang, B. Jiang, J. Ma, R. Dawes, D. Xie, J. M. Bowman and H. Guo, J. Chem. Phys. **136**, 041103 (2012).
74 J. Li, C. Xie, J. Ma, Y. Wang, R. Dawes, D. Xie, J. M. Bowman and H. Guo, J. Phys. Chem. A **116**, 5057 (2012).
75 J. Li, R. Dawes and H. Guo, J. Chem. Phys. **137**, 094304 (2012).
76 J. Li, B. Jiang and H. Guo, J. Chem. Phys. **138**, 074309 (2013).
77 J. Li and H. Guo, J. Chem. Phys **138**, 194304 (2013).
78 J. Li, R. Dawes and H. Guo, J. Chem. Phys. **139**, 074302 (2013).
79 C. M. Handley and P. L. A. Popelier, J. Phys. Chem. A **114**, 3371 (2010).
80 J. Behler, Phys. Chem. Chem. Phys. **13**, 17930 (2011).
81 L. M. Raff, R. Komanduri, M. Hagan and S. T. S. Bukkapatnam, *Neural Networks in Chemical Reaction Dynamics*. (Oxford University Press, Oxford, 2012).
82 J. Chen, X. Xu and D. H. Zhang, J. Chem. Phys. **138**, 154301 (2013).
83 Z. Xie and J. M. Bowman, J. Chem. Theo. Comp. **6**, 26 (2010).
84 B. J. Braams and J. M. Bowman, Int. Rev. Phys. Chem. **28**, 577 (2009).
85 W. Lai, S. Y. Lin, D. Xie and H. Guo, J. Chem. Phys. **129**, 154311 (2008).
86 W. H. Miller, N. C. Handy and J. E. Adams, J. Chem. Phys. **72**, 99 (1980).
87 J. C. Corchado, Y.-Y. Chuang, P. L. Fast, W.-P. Hu, Y.-P. Liu, G. C. Lynch, K. A. Nguyen, C. F. Jackels, A. Fernandez Ramos, B. A. Ellingson, B. J. Lynch, J. Zheng, V. S. Melissas, J. Villà, I. Rossi, E. L. Coitiño, J. Pu, T. V. Albu, R. Steckler, B. C. Garrett, A. D. Isaacson and D. G. Truhlar, (University of Minnesota, Minneapolis, 2007).
88 M. Page and J. W. McIver, J. Chem. Phys. **88**, 922 (1988).
89 Y.-Y. Chuang and D. G. Truhlar, J. Phys. Chem. A **102**, 242 (1998).
90 D. G. Truhlar, A. D. Issacson and B. C. Garrett, in *Theory of Chemical Reaction Dynamics*, edited by M. Bear (CRC, Boca Raton, 1985), pp. 65-137.
91 W. L. Hase, R. J. Duchovic, X. Hu, A. Komornicki, K. F. Lim, D.-H. Lu, G. H. Peslherbe, K. N. Swamy, S. R. V. Linde, A. Varandas, H. Wang and R. J. Wolf, Quantum Chemistry Program Exchange Bulletin **16**, 671 (1996).
92 X. Hu, W. L. Hase and T. Pirraglia, J. Comp. Chem. **12**, 1014 (1991).
93 B. Jiang and H. Guo, J. Chem. Phys. **138**, 234104 (2013).
94 B. Jiang and H. Guo, J. Am. Chem. Soc. **135**, 15251 (2013).

95 B. Jiang, J. Li and H. Guo, J. Chem. Phys. **140**, 034112 (2014).
96 B. Jiang, R. Liu, J. Li, D. Xie, M. Yang and H. Guo, Chem. Sci. **4**, 3249 (2013).
97 B. Jiang and H. Guo, J. Phys. Chem. C **117**, 16127 (2013).

Table I. Comparison of the geometries (Å for bond lengths and ° for angles) of the stationary points for the ground electronic state of $NH_4$.

| Species | Level | Geometry | | | | | |
|---|---|---|---|---|---|---|---|
| | | $R_{HH'}$ | | | | | |
| $H_2$ ($D_{\infty h}$) | PIP-NN PES [a] | 0.7417 | | | | | |
| | FC-F12a/AVDZ [b] | 0.7459 | | | | | |
| | FC-F12a/AVTZ [c] | 0.7419 | | | | | |
| | AE-F12b/VDZ-F12 [d] | 0.7419 | | | | | |
| | AE-F12b/VTZ-F12 [e] | 0.7417 | | | | | |
| | AE-F12b/VQZ-F12 [f] | 0.7415 | | | | | |
| | Expt. [g] | 0.741 | | | | | |
| | | $R_{NH}$ | $\theta_{HNH'}$ | | | | |
| $NH_2$ ($C_{2v}$) | PIP-NN PES | 1.0250 | 103.17 | | | | |
| | FC-F12a/AVDZ | 1.0265 | 102.97 | | | | |
| | FC-F12a/AVTZ | 1.0251 | 103.05 | | | | |
| | AE-F12b/VDZ-F12 | 1.0240 | 103.00 | | | | |
| | AE-F12b/VTZ-F12 | 1.0237 | 103.12 | | | | |
| | AE-F12b/VQZ-F12 | 1.0234 | 103.17 | | | | |
| | Expt. | 1.024 | 103.4 | | | | |
| | CE-2010 [h] | 1.012 | 103.4 | | | | |
| | | $R_{NH}$ | $\theta_{HNH'}$ | | | | |
| $NH_3$ ($C_{3v}$) | PIP-NN PES | 1.0125 | 106.62 | | | | |
| | FC-F12a/AVDZ | 1.0135 | 106.62 | | | | |
| | FC-F12a/AVTZ | 1.0124 | 106.61 | | | | |
| | AE-F12b/VDZ-F12 | 1.0111 | 106.75 | | | | |
| | AE-F12b/VTZ-F12 | 1.0110 | 106.76 | | | | |
| | AE-F12b/VQZ-F12 | 1.0107 | 106.80 | | | | |
| | Expt. | 1.012 | 106.67 | | | | |
| | CE-2010 | 1.012 | 109.0 | | | | |
| | | $R_{NH}$ | | | | | |
| $NH_4$ ($T_d$) | PIP-NN PES | 1.0388 | | | | | |
| | FC-F12a/AVDZ | 1.0399 | | | | | |
| | FC-F12a/AVTZ | 1.0388 | | | | | |
| | AE-F12b/VDZ-F12 | 1.0383 | | | | | |
| | AE-F12b/VTZ-F12 | 1.0382 | | | | | |
| | FC/VTZ [i] | 1.0520 | | | | | |
| | FC/VQZ [j] | 1.0457 | | | | | |
| | MRCI+$Q_r$/AVDZ [k] | 1.0494 | | | | | |
| | MRCI+$Q_r$/AVTZ [l] | 1.0425 | | | | | |
| | Expt. [m] | 1.0365 | | | | | |
| | CCSD(T)/CBS [n] | 1.0355 | | | | | |
| | | $R_{NH}$ | | | | | |
| $NH_3$-TS ($D_{3h}$) | PIP-NN PES | 0.9958 | | | | | |
| | FC-F12a/AVDZ | 0.9968 | | | | | |
| | FC-F12a/AVTZ | 0.9958 | | | | | |
| | AE-F12b/VDZ-F12 | 0.9946 | | | | | |
| | AE-F12b/VTZ-F12 | 0.9946 | | | | | |
| | AE-F12b/VQZ-F12 | 0.9945 | | | | | |
| | CE-2010 | 1.012 | | | | | |
| | | $R_{H''H'}$ | $R_{NH'}$ | $\theta_{NH'H''}$ | $R_{NH}$ | $\theta_{HNH'}$ | $\phi_{HNH'H''}$ |
| TS1 ($C_s$) | PIP-NN PES | 0.8804 | 1.3239 | 159.16 | 1.0244 | 97.89 | 52.42 |
| | FC-F12a/AVDZ | 0.8843 | 1.3246 | 160.24 | 1.0251 | 98.14 | 52.62 |
| | FC-F12a/AVTZ | 0.8817 | 1.3216 | 159.96 | 1.0238 | 98.10 | 52.63 |
| | AE-F12b/VDZ-F12 | 0.8817 | 1.3218 | 159.98 | 1.0226 | 98.16 | 52.67 |
| | AE-F12b/VTZ-F12 | 0.8811 | 1.3222 | 159.79 | 1.0224 | 98.17 | 52.70 |
| | CE-2010 | 0.868 | 1.279 | 180.0 | 1.013 | - | - |

| | | | | | | | |
|---|---|---|---|---|---|---|---|
| | CCSD(T) [o] | 0.890 | 1.307 | 158.7 | 1.022 | 98.5 | |
| | | $R_{NH'}$ | $R_{NH}$ | $\theta_{HNH'}$ | $\phi_{HNH'H}$ | | |
| TS2 ($C_{3v}$) | PIP-NN PES | 1.4101 | 1.0193 | 109.67 | 120.25 | | |
| | FC-F12a/AVDZ | 1.4127 | 1.0206 | 109.56 | 120.00 | | |
| | FC-F12a/AVTZ | 1.4092 | 1.0195 | 109.55 | 120.00 | | |
| | AE-F12b/VDZ-F12 | 1.3925 | 1.0181 | 109.45 | 120.00 | | |
| | AE-F12b/VTZ-F12 | 1.3965 | 1.0183 | 109.50 | 120.00 | | |

[a]: Fitted PES, this work; [b]: FC-(U)CCSD(T)-F12a/AVDZ, this work; [c]: FC-(U)CCSD(T)-F12a/AVTZ, this work; [d]: AE-(U)CCSD(T)-F12b/cc-pCVDZ-F12, this work; [e]: AE-(U)CCSD(T)-F12b/cc-pCVTZ-F12, this work; [f]: AE-(U)CCSD(T)-F12b/cc-pCVQZ-F12, this work; [g]: see http://cccbdb.nist.gov/; [h]: Ref. 26; [i]: FC-UCCSD(T)/cc-pVTZ, this work; [j]: FC-UCCSD(T)/cc-pVQZ, this work; [k]: 2-state-MRCI+$Q_{rot}$/AVDZ, this work; [l]: 2-state-MRCI+$Q_{rot}$/AVTZ, this work; [m]: Ref. 53; [n]: extrapolated from energies at CCSD(T)/AVXZ (X=D, T, Q and 5), Ref. 58; [o]: CCSD(T)/[5s4p3d/4s3p], Ref. 23.

Table II. Comparison of the calculated harmonic vibrational frequencies ($cm^{-1}$) of the stationary points in the $NH_4$ system.* The experimental ones include anharmonicity.

| Species | Level | Frequencies ($cm^{-1}$) | | | | | | | | |
|---|---|---|---|---|---|---|---|---|---|---|
| | | 1 | 2 | 3 | 4 | 5 | 6 | 7 | 8 | 9 |
| $H_2$ ($D_{\infty h}$) | PIP-NN PES [a] | 4402 | | | | | | | | |
| | FC-F12a/AVDZ [b] | 4385 | | | | | | | | |
| | FC-F12a/AVTZ [c] | 4401 | | | | | | | | |
| | AE-F12b/VDZ-F12 [d] | 4405 | | | | | | | | |
| | AE-F12b/VTZ-F12 [e] | 4401 | | | | | | | | |
| | AE-F12b/VQZ-F12 [f] | 4404 | | | | | | | | |
| | Expt. [g] | 4359 | | | | | | | | |
| $NH_2$ ($C_{2v}$) | | ($\nu_1$, $A_1$) | ($\nu_2$, $A_1$) | ($\nu_2$, $B_2$) | | | | | | |
| | PIP-NN PES [a] | 3379 | 1549 | 3469 | | | | | | |
| | FC-F12a/AVDZ [b] | 3371 | 1538 | 3466 | | | | | | |
| | FC-F12a/AVTZ [c] | 3375 | 1541 | 3470 | | | | | | |
| | AE-F12b/VDZ-F12 [d] | 3383 | 1547 | 3478 | | | | | | |
| | AE-F12b/VTZ-F12 [e] | 3384 | 1545 | 3480 | | | | | | |
| | AE-F12b/VQZ-F12 [f] | 3386 | 1544 | 3483 | | | | | | |
| | Expt. [g] | 3219 | 1497 | 3301 | | | | | | |
| | CE-2010 [h] | 3395 | 1462 | 3443 | | | | | | |
| $NH_3$ ($C_{3v}$) | | ($\nu_1$, $A_1$) | ($\nu_2$, $A_1$) | ($\nu_3$, E) | ($\nu_4$, E) | | | | | |
| | PIP-NN PES [a] | 3478 | 1056 | 3608 | 1674 | | | | | |
| | FC-F12a/AVDZ [b] | 3477 | 1052 | 3609 | 1668 | | | | | |
| | FC-F12a/AVTZ [c] | 3477 | 1055 | 3609 | 1673 | | | | | |
| | AE-F12b/VDZ-F12 [d] | 3490 | 1055 | 3621 | 1681 | | | | | |
| | AE-F12b/VTZ-F12 [e] | 3487 | 1050 | 3620 | 1676 | | | | | |
| | AE-F12b/VQZ-F12 [f] | 3489 | 1050 | 3622 | 1676 | | | | | |
| | Expt. [g] | 3337 | 950 | 3444 | 1627 | | | | | |
| | CE-2010 [h] | 3478 | 1112 | 3606 | 1630 | | | | | |
| $NH_4$ ($T_d$) | | ($\nu_1$, $A_1$) | ($\nu_2$, E) | ($\nu_3$, $T_2$) | ($\nu_4$, $T_2$) | | | | | |
| | PIP-NN PES [a] | 3032 | 1620 | 3077 | 1326 | | | | | |
| | FC-F12a/AVDZ [b] | 3045 | 1609 | 3074 | 1317 | | | | | |
| | FC-F12a/AVTZ [c] | 3048 | 1613 | 3073 | 1323 | | | | | |
| | AE-F12b/VDZ-F12 [d] | 3040 | 1681 | 3046 | 1318 | | | | | |
| | AE-F12b/VTZ-F12 [e] | 3042 | 1641 | 3063 | 1319 | | | | | |
| | AE-F12b/VQZ-F12 [f] | 3042 | 1669 | 3059 | 1339 | | | | | |
| | FC/VTZ [i] | 2728 | 1536 | 2728 | 1231 | | | | | |
| | FC/VQZ [j] | 2867 | 1565 | 2868 | 1260 | | | | | |
| | Expt.[p] | 2552 | 1581 | | | | | | | |
| $NH_3$-TS ($D_{3h}$) | PIP-NN PES [a] | 842i | 1583 | 3631 | 3845 | | | | | |
| | FC-F12a/AVDZ [b] | 836i | 1585 | 3633 | 3847 | | | | | |
| | FC-F12a/AVTZ [c] | 845i | 1583 | 3633 | 3846 | | | | | |
| | AE-F12b/VDZ-F12 [d] | 848i | 1590 | 3645 | 3857 | | | | | |
| | AE-F12b/VTZ-F12 [e] | 845i | 1586 | 3642 | 3854 | | | | | |
| | AE-F12b/VQZ-F12 [f] | 839i | 1586 | 3642 | 3855 | | | | | |
| | CE-2010 [h] | 903i | 1812 | 3422 | 3622 | | | | | |
| TS1 ($C_s$) | PIP-NN PES [a] | 1569i | 650 | 692 | 1095 | 1196 | 1552 | 1975 | 3401 | 3489 |
| | FC-F12a/AVDZ [b] | 1557i | 645 | 670 | 1079 | 1199 | 1543 | 1967 | 3389 | 3486 |
| | FC-F12a/AVTZ [c] | 1590i | 648 | 677 | 1086 | 1206 | 1549 | 1960 | 3393 | 3490 |
| | AE-F12b/VDZ-F12 [d] | 1557i | 649 | 674 | 1089 | 1214 | 1553 | 1963 | 3403 | 3500 |
| | AE-F12b/VTZ-F12 [e] | 1575i | 650 | 678 | 1086 | 1207 | 1552 | 1968 | 3403 | 3501 |
| | CCSD(T) [o] | 1624i | 672 | 704 | 1125 | 1277 | 1576 | 1908 | 3390 | 3485 |
| | CE-2010 | 1602i | 581 | 622 | 1080 | 1497 | 1623 | 1861 | 3373 | 3444 |
| TS2 ($C_{3v}$) | PIP-NN PES [a] | 1623i | 612 | 1119 | 1608 | 3323 | 3511 | | | |
| | FC-F12a/AVDZ [b] | 1572i | 612 | 1118 | 1614 | 3319 | 3512 | | | |
| | FC-F12a/AVTZ [c] | 1616i | 611 | 1122 | 1620 | 3321 | 3514 | | | |
| | AE-F12b/VDZ-F12 [d] | 1741i | 638 | 1134 | 1649 | 3335 | 3521 | | | |
| | AE-F12b/VTZ-F12 [e] | 1733i | 620 | 1121 | 1631 | 3326 | 3519 | | | |

*: See the notations in Table I. [p]: Ref. 49.

Table III. Comparison of the energies (kcal/mol, all relative to *ab initio* energy of H + $NH_3$) of the stationary points in the $NH_4$ system. [*]

| | H+$NH_3$ | TS1 | $H_2$+$NH_2$ | TS2 | $NH_4$ |
|---|---|---|---|---|---|
| PIP-NN PES [a] | 0.00 | 15.11 | 5.65 | 9.43 | -2.38 |
| FC-CCSD(T)-F12a/AVDZ [b] | 0 | 15.21 | 5.86 | 9.16 | -2.54 |
| FC-CCSD(T)-F12a/AVTZ [c] | 0 | 15.20 | 5.65 | 9.39 | -2.37 |
| MRCI+Q(FV)/AVDZ [d] | 0 | 11.95 | 2.74 | 7.66 | -3.11 |
| MRCI+Q(FV)/AVTZ [e] | 0 | 11.14 | 1.53 | 7.07 | -3.86 |
| MRCI+Q(FV)/AVQZ [f] | 0 | 11.60 | 2.11 | 7.24 | -3.68 |
| MRCI+Q(FV+3s)/AVDZ [g] | 0 | 14.22 | 4.35 | 8.76 | -2.24 |
| MRCI+Q(FV+3s)/AVTZ [h] | 0 | 14.28 | 4.08 | 8.93 | -2.20 |
| MRCI+Q(FV+3s)/AVQZ [i] | 0 | 14.68 | 4.63 | 9.02 | -2.07 |
| MRCI+Q(FV+3s)/CBS-DT [j] | 0 | 14.31 | 3.97 | 9.01 | -2.18 |
| MRCI+Q(FV+3s)/CBS-TQ [k] | 0 | 14.96 | 5.02 | 9.08 | -1.98 |
| MRCI+Q(FV+3s)/ROOS [l] | 0 | 14.58 | 4.81 | 9.07 | -2.20 |
| MRCI+Q(FV+3s3p)/AVDZ [m] | 0 | 14.36 | 5.08 | 9.38 | -2.11 |
| CCSD(T) [n] | 0 | 15.40 | 6.39 | - | - |
| PES-1997 [o] | 0 | 15.75 | 6.0 | - | - |
| PES-2009 [p] | 0 | 14.48 | 5.0 | - | - |
| MC PES [q] | 0 | 15.06 | 5.71 | 9.30 | -2.41 |
| HEAT [r] | 0 (0) | | 5.99 (5.98) | | |

[*]: See also notations in Tables I and II; [j], results extrapolated from [g](AVDZ) and [h](AVTZ); [k]: results extrapolated from [h](AVTZ) and [i](AVQZ); [n]: Ref. 23; [o]: Ref. 25; [p]: Ref. 26; [q]: Ref. 27. [r]: Ref. 70, values in parentheses include small corrections such as relativistic and diagonal Born-Oppenheimer corrections.

Table IV. Kinetic isotope effects for the abstraction reaction and its reverse. The square brackets in the experimental column denote extrapolated data.

| R1 | | | | | R-1 | | |
|---|---|---|---|---|---|---|---|
| T/K | Expt. [a] | CE-1997 [b] | CE-2010 [b] | PIP-NN PES [c] | CE-2010 [b] | CE-1997 [b] | PIP-NN PES [c] |
| 500 | [2.46] | 3.51 | 2.87 | 3.81 | 2.35 | 2.46 | 3.00 |
| 600 | 2.32 | 2.83 | 2.48 | 3.01 | 2.21 | 2.22 | 2.60 |
| 700 | 2.25 | 2.45 | 2.24 | 2.58 | 2.10 | 2.06 | 2.35 |
| 1000 | 2.1 | 1.92 | 1.87 | 1.97 | 1.87 | 1.79 | 1.93 |
| 1200 | 2.04 | 1.75 | 1.75 | 1.79 | 1.77 | 1.68 | 1.78 |
| 1500 | [1.97] | 1.61 | 1.54 | 1.63 | 1.66 | 1.58 | 1.64 |

[a]: see Ref. 26 and references cited therein; [b]: Ref. 26; [c]: This work.

Table V. SVP projections (averaged values used for degenerate modes) of the vibrations of the reactants ($H+NH_3$) and products ($H_2+NH_2$) for the abstraction reaction $H+NH_3 \rightarrow H_2+NH_2$ on the PIP-NN PES.

| $H+NH_3$ | | $H_2+NH_2$ | |
|---|---|---|---|
| Mode | $P_i$ | Mode | $P_i$ |
| $NH_3$ symmetric stretch, $\nu_1$ ($A_1$) | 0.560 | H-H stretch | 0.648 |
| $NH_3$ umbrella, $\nu_2$ ($A_1$) | 0.132 | $NH_2$ symmetric stretch | 0.003 |
| $NH_3$ asymmetric stretch, $\nu_3$ (E) | 0.576 | $NH_2$ asymmetric stretch | 0.004 |
| $NH_3$ bend, $\nu_4$ (E) | 0.048 | $NH_2$ bend | 0.003 |

**Figure captions:**

Figure 1. Schematic illustration of the abstraction and exchange/association reaction energetics and stationary point geometries. The energies are in kcal/mol relative to the $NH_3$ + H, and the data in parentheses are the corresponding zero-point energies within the harmonic oscillator approximation.

Figure 2. Comparison of the minimum energy paths for the $NH_3$ inversion (upper panel), abstraction (middle panel), and the exchange/association paths (lower panel) for $NH_4$. The *ab initio* values are in symbols and PES in lines. Energies are in kcal/mol relative to the reactant asymptote H + $NH_3$.

Figure 3. Fitting errors ($E_{\rm fit}$-$E_{\rm ab\ inito}$) using the PIP-NN method as a function of the energy.

Figure 4. Potential energy dependence with respect to the NHH angle with other coordinates fixed at the optimized TS1 geometry (upper panel) and one-dimensional PES plot along $R_{\rm NH}$ with other coordinates fixed at the $NH_4$ equilibrium (lower panel). The *ab initio* values are in squares and PES in lines.

Figure 5. Potential energy surface as a function of the $r_{\rm NH}$ and $r_{\rm HH}$ distances while all other coordinates are optimized. The maximum of the energy is 30 kcal/mol with a contour interval 3 kcal/mol.

Figure 6. Minimum energy path, $V_{\rm MEP}$, zero point energy, ZPE, and vibrationally adiabatic ground state energy $V_a^G$ (all energies in kcal/mol) as a function of the reaction coordinate *s* (upper panel), generalized normal mode vibrational frequencies ($10^3$ $cm^{-1}$) as a function of *s*

(middle panel), and the reaction path curvature, $\kappa$ in $amu^{-1/2}bohr^{-1}$ (lower panel)

Figure 7. Canonical rate constants for the forward directions of the abstraction reactions $H+NH_3 \rightarrow H_2+NH_2$ (upper panel, QCT results using the PIP-NN PES in squares) and $D+ND_3 \rightarrow D_2+ND_2$ (lower panel) with comparison to the available experimental values.[40, 42]

Figure 8. Canonical rate constants for the reverse directions of the abstraction reactions $H+NH_3 \rightarrow H_2+NH_2$ (upper panel) and $D+ND_3 \rightarrow D_2+ND_2$ (lower panel) with comparison to the available experimental values.[43-45]

Figure 1

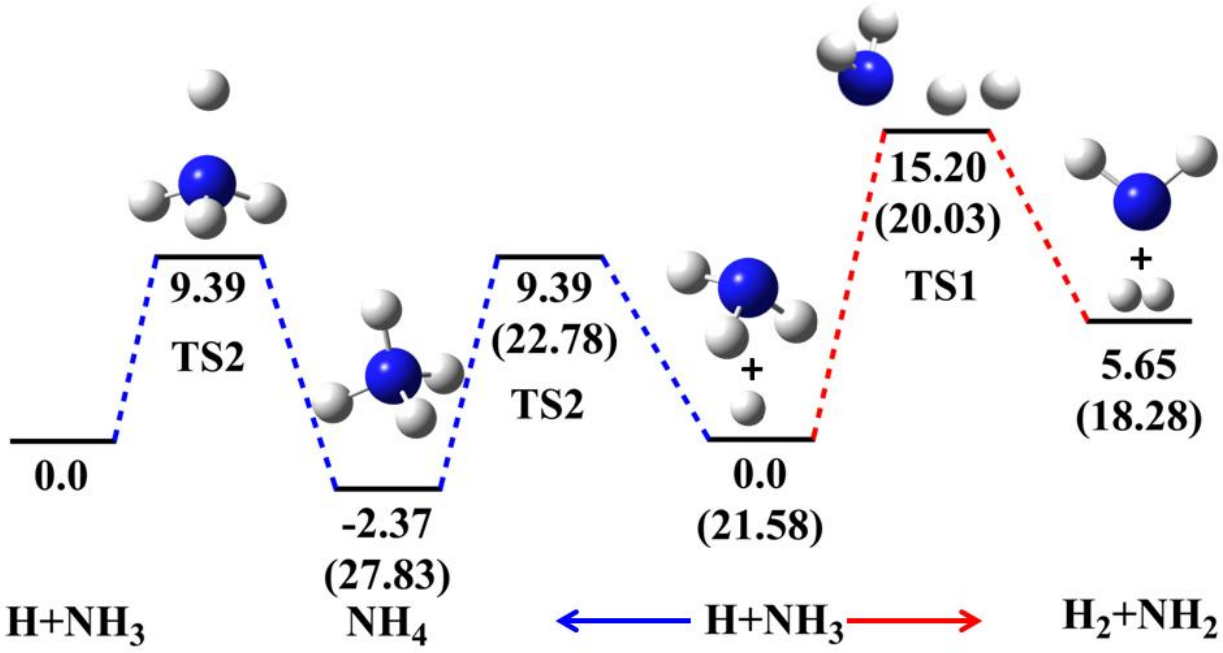

Figure 2

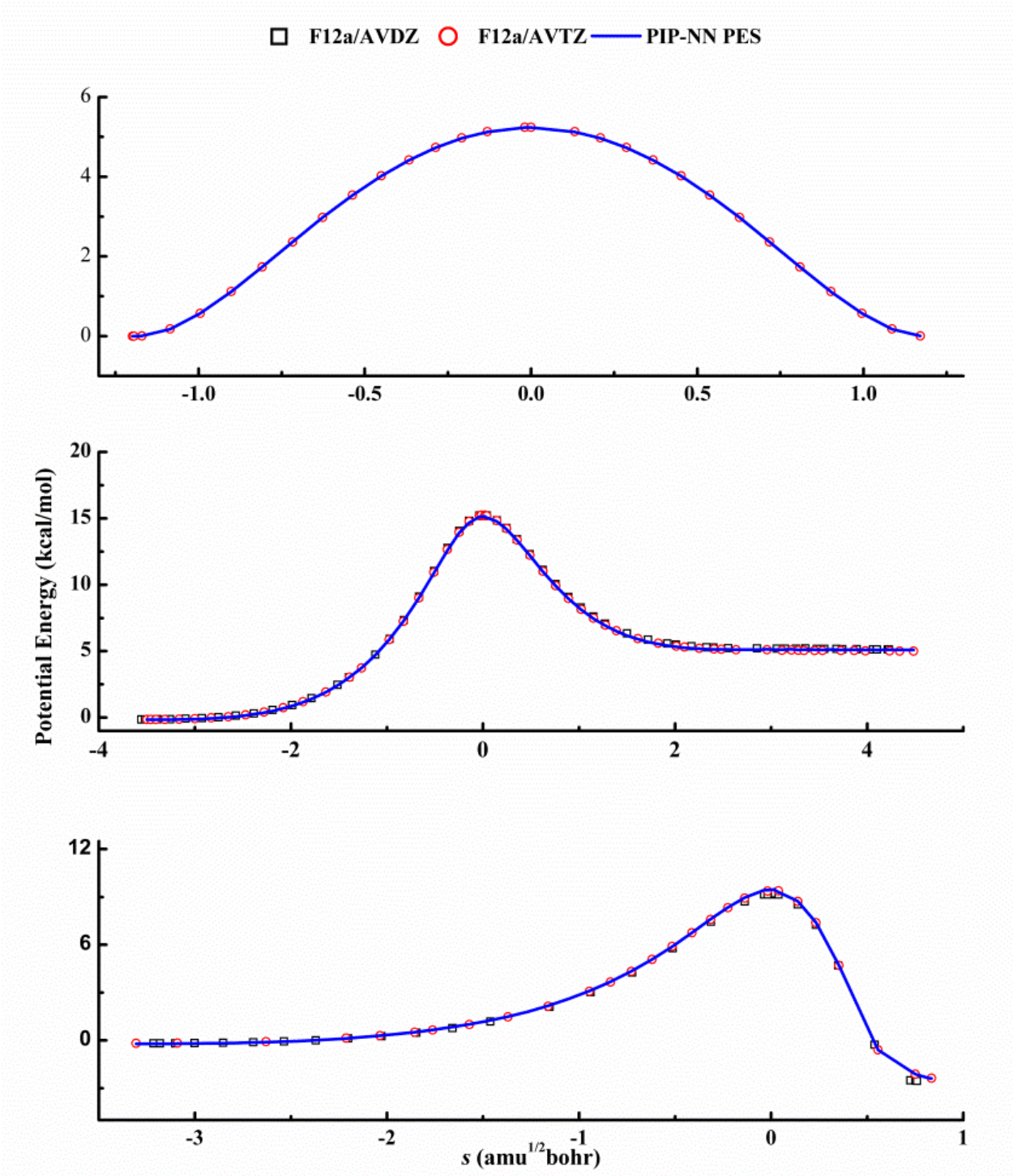

Figure 3

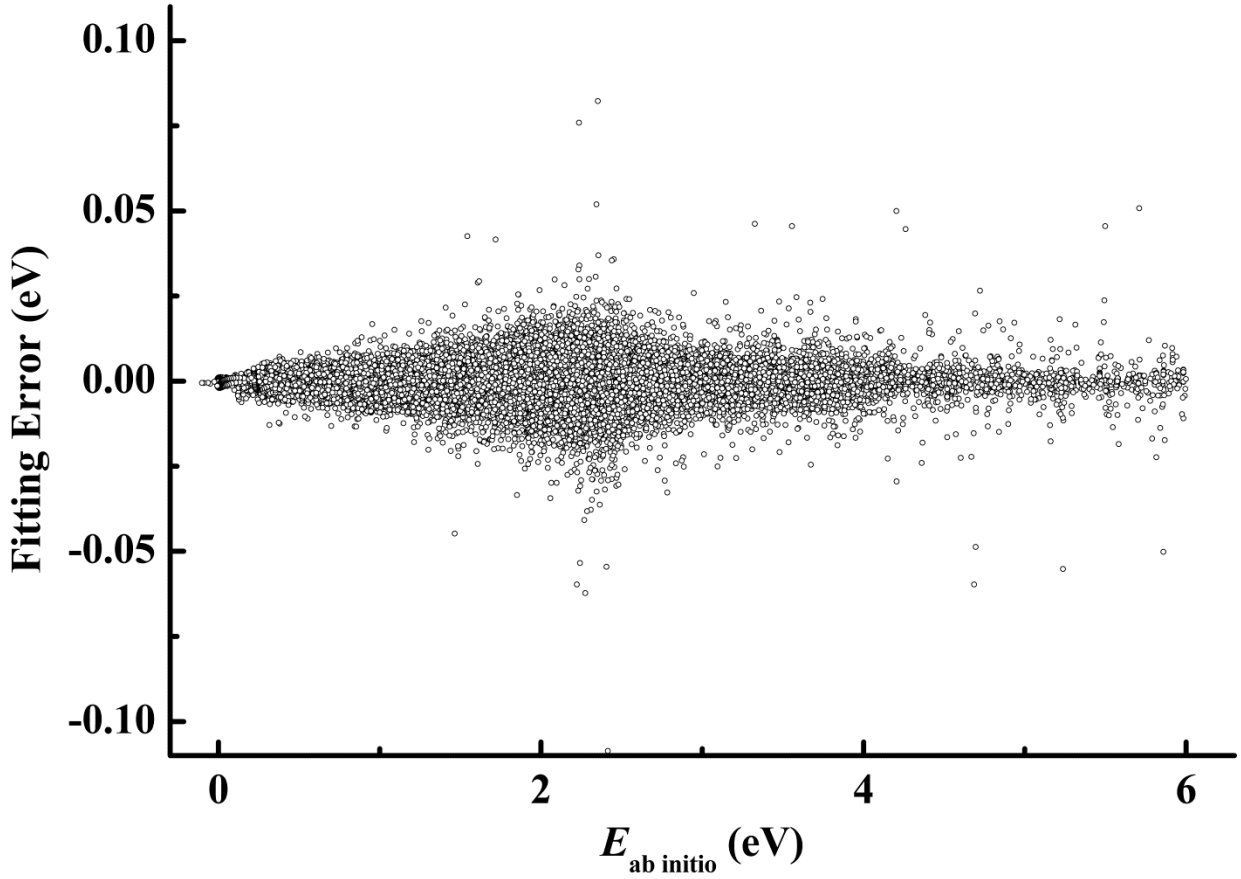

Figure 4

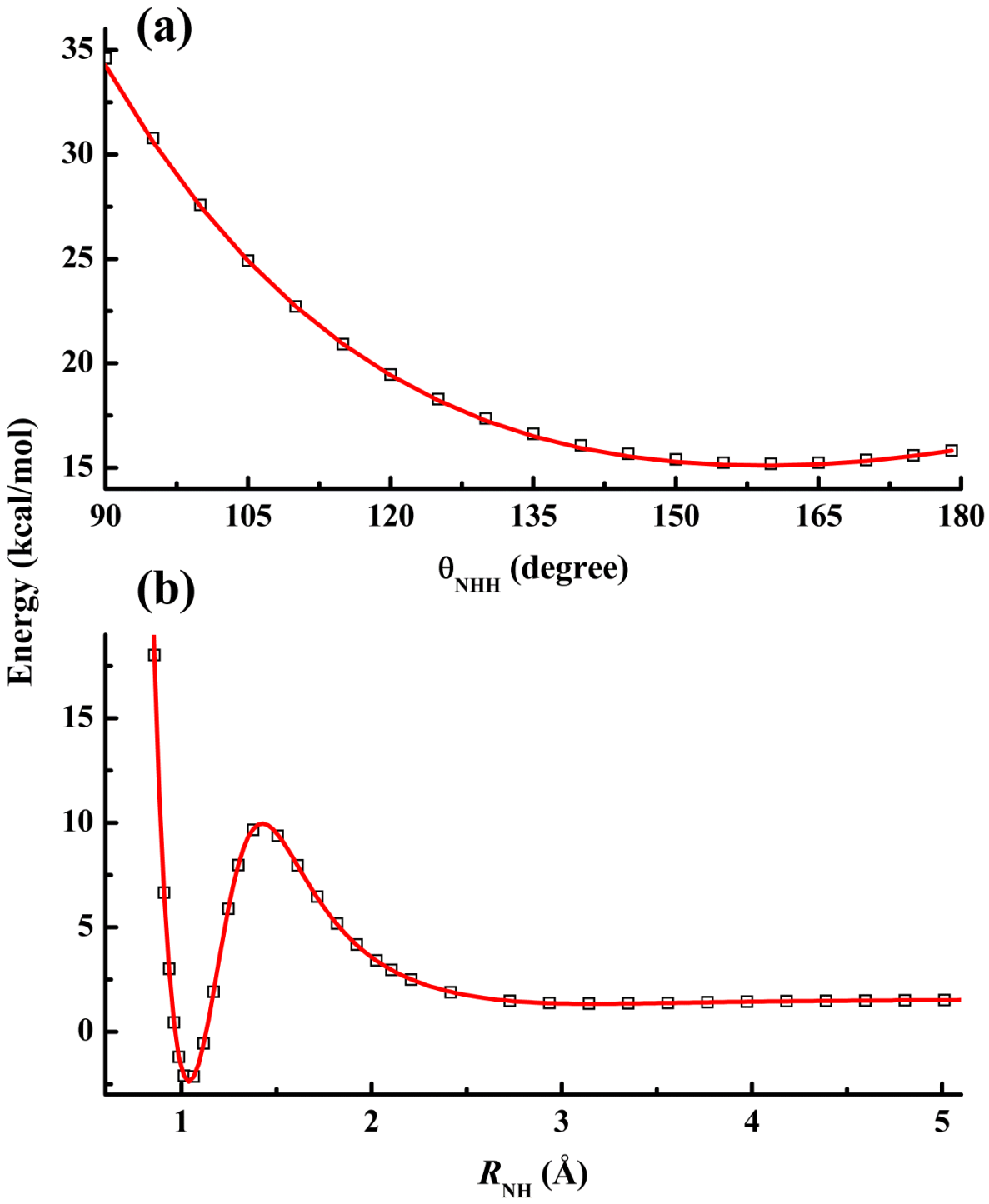

Figure 5

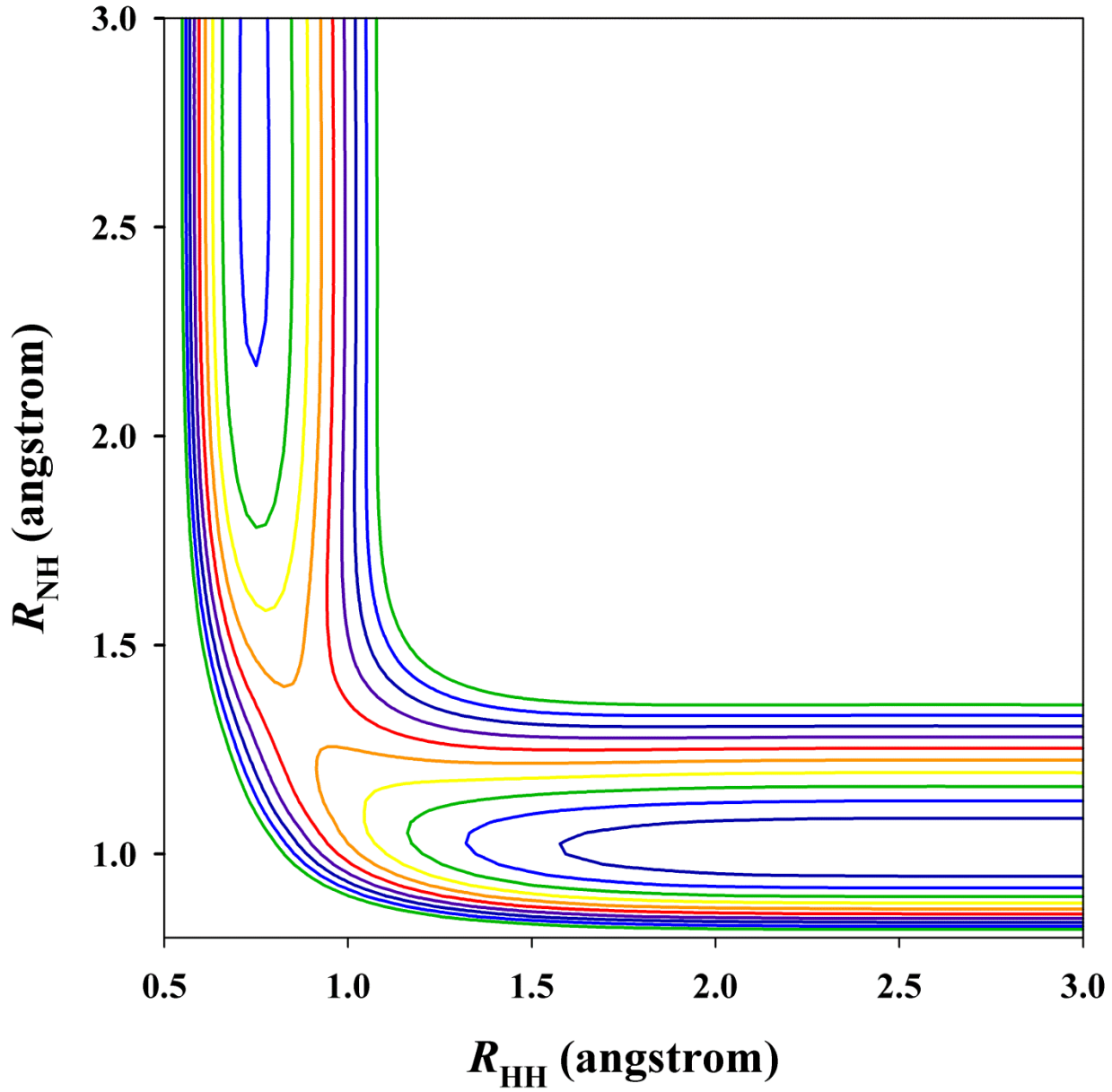

Figure 6

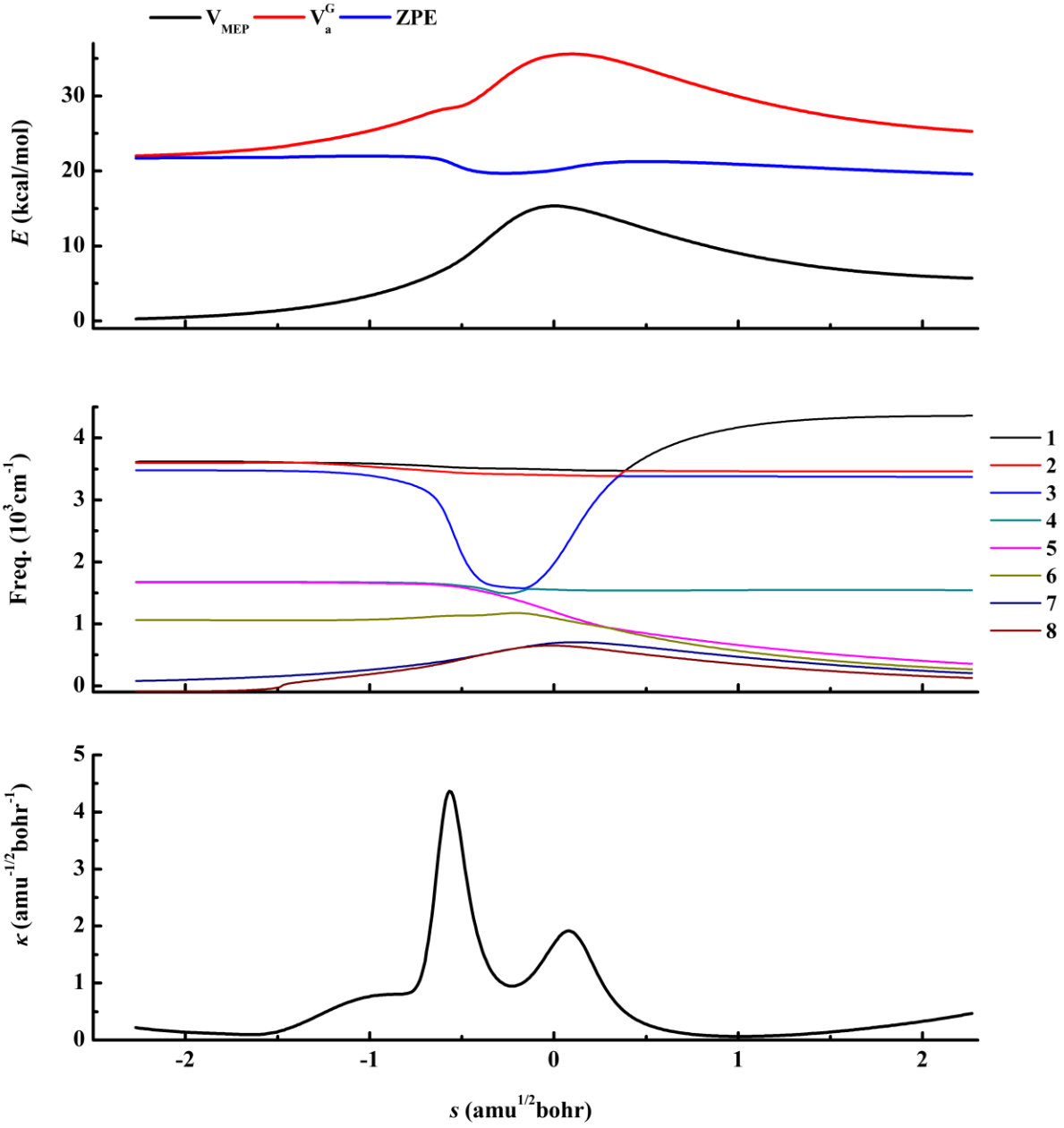

Figure 7

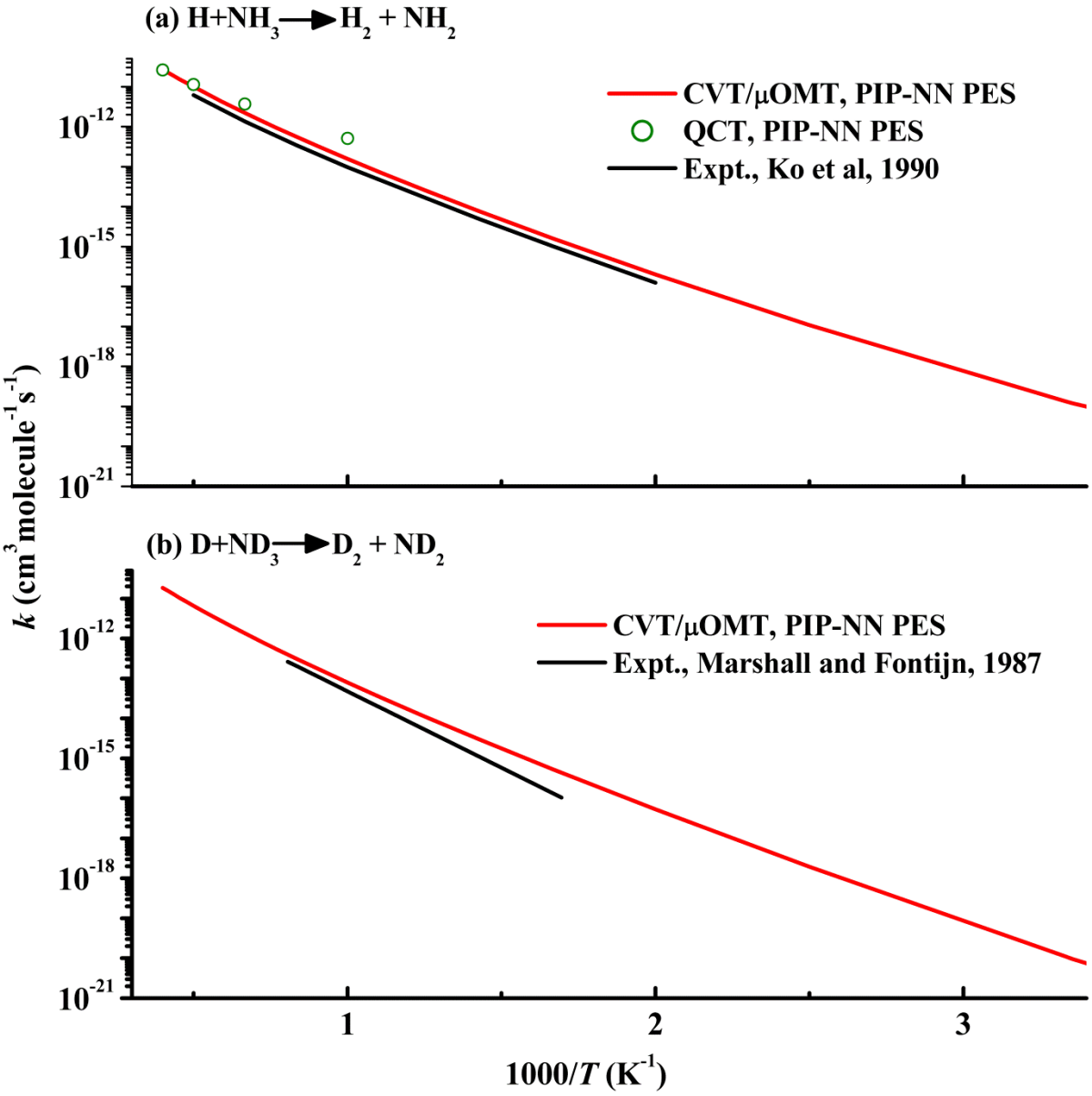

Figure 8